PHILOSOPHICAL TRANSACTIONS OF THE ROYAL SOCIETY A MATHEMATICAL, PHYSICAL & ENGINEERING SCIENCES

The Structure of the Turbulent Atmospheric Boundary Layer [and Discussion]

S. Nicholls, B. Brummer, F. Fiedler, A. Grant, T. Hauf, G. Jenkins, C. Readings, W. Shaw, P. K. Taylor, J. A. Businger and J. D. Woods

Phil. Trans. R. Soc. Lond. A 1983 **308**, 291-309
doi: 10.1098/rsta.1983.0005

Phil. Trans. R. Soc. Lond. A **308**, 291–309 (1983)
Printed in Great Britain

The structure of the turbulent atmospheric boundary layer

By S. Nicholls†, B. Brümmer‡, F. Fiedler§, A. Grant‖, T. Hauf§, G. Jenkins‖, C. Readings‖ and W. Shaw¶

† *Meterological Research Flight, R.A.E., Farnborough, Hants, U.K.*
‡ *Max Planck Institut für Meteorologie, Hamburg, F.R.G.*
§ *Meteorologisches Institut, University of Karlsruhe, F.R.G.*
‖ *Meteorological Office, Bracknell, Berks RG12 2SZ, U.K.*
¶ *Dept of Atmospheric Sciences, University of Washington, Seattle, Washington* 98195, *U.S.A.*

During the Joint Air–Sea Interaction Experiment (JASIN), mean flow and turbulent fluctuations were measured throughout the depth of the atmospheric boundary layer by shipborne surface instrumentation, multiple-instrument packages suspended from tethered balloons and research aircraft flying in low level formation. These enabled both individual localized events and representative area-average (70 km × 70 km) measurements to be investigated.

The results are summarized and show that continuous small-scale turbulent mixing was generally confined to an Ekman layer a few hundred metres deep. The structure of this layer is examined in detail, particularly the momentum balance. Spectral analysis reveals two energy-containing regions, one of which, at higher wavenumbers, scales with the Ekman layer depth and carries most of the vertical fluxes. Direct coupling between the Ekman layer and the overlying atmosphere is weak and appears to be strongly dependent on cloud processes, which are intermittent and irregularly distributed on the scale of these measurements.

1. Introduction

Interaction between the large-scale atmospheric circulation and the Earth's surface takes place within the atmospheric boundary layer (BL). However, as the resulting flow is almost always turbulent, the problem of determining the structure of the BL necessitates a statistical approach. The resultant governing equations cannot be solved exactly, so calculations of BL characteristics depend on various simplifying assumptions and approximations. Unfortunately, it is difficult to assess the validity of such methods as the solutions are often strongly dependent on the details of these assumptions, which are often difficult to justify theoretically. Thus much of our present understanding of the BL is based on observational results.

The structure of the BL is often discussed in terms of similarity theories (see for example the review by McBean (1979)), which can provide an elegant, universal description as well as a framework for the analysis of data and comparison of results. However, these remain valid only under certain restricted conditions, and observations are needed to test their utility and to establish actual numerical values of functions that similarity theories alone cannot predict. JASIN data can be used to evaluate critically certain aspects of these theories and also to assess the effects of physical processes that are not currently considered by such schemes (e.g. the effects of cloud, mesoscale (10 km–100 km) variability and radiation).

The advent of modern instrumentation and fast data processing techniques has recently

resulted in a greatly increased number of observational investigations into the structure and dynamics of the BL. Most of these have been concentrated in the lowest few metres of the atmosphere over land surfaces, which are fairly amenable to investigation. As a result, many aspects of this part of the BL are now well documented (see for example reviews by Busch (1973), Businger (1973) and Wyngaard (1973)). Measurements made throughout the depth of the BL are much more limited, especially over open sea where conditions are typically quite different from those found over land, for example convection and diurnal forcing are usually much weaker and the effects of water vapour more predominant. Furthermore, the few investigations of this type that have been made tend to fall into two groups: those based on mean flow data from which certain properties of the turbulent mixing processes may be deduced (see for example Brümmer *et al.* 1974, Clarke & Hess 1974) and those in which direct measurements of turbulent fluctuations were made with the accurate determination of the mean flow a secondary consideration (see for example Kaimal *et al.* 1976, Caughey & Palmer 1979, Nicholls & Readings 1981). The sampling requirements of the former can only be met by long averaging times, often days, which generally restricts the use of such methods to particularly steady, uniform situations. Otherwise, the interpretation of the results becomes difficult. The latter suffer from an ill defined description of the mean flow caused either by insufficiently accurate measurements or limited sampling so that the directly measured turbulent fluxes cannot readily be related to the large-scale flow. This division has resulted in some tests of predictions or hypotheses concerning BL structure being inconclusive since simultaneous measurements of both turbulent quantities and the mean flow are often required. These problems were minimized during JASIN by a combination of low-level flights by several aircraft in formation, observations made from instrument packages suspended from tethered balloons and surface-based instrumentation. On a large scale, comprehensive mean flow measurements were provided by radiosondes, but results from these are presented elsewhere (Taylor *et al.* this symposium).

(*a*) *Notation*

$\mathrm{Co}_{xy}(k)$	cospectrum of x and y
f	Coriolis parameter
E	turbulent kinetic energy $\equiv \frac{1}{2}(u'^2+v'^2+w'^2)$
G	geostrophic wind-speed
k	wavenumber ($\equiv$ wavelength^{-1})
κ	Von Karman constant (taken as 0.4)
L	Monin–Obukhov length $= -u_*^3 T_\mathrm{v}(g\kappa\overline{w' T'_{\mathrm{v},0}})^{-1}$
L_v	latent heat of vaporization of water
p	pressure
Q	specific humidity
Q_l	specific liquid water content
$S_x(k)$	spectrum of x
T	temperature
T_v	virtual temperature
u, v, w or U, V, W	wind components
u_*	$(-\overline{u'w'_0})^{\frac{1}{2}}$
z	geometric altitude

z_0 surface roughness length
ϵ rate of dissipation of turbulent kinetic energy
Θ_v, Θ_e virtual and equivalent potential temperature
ρ density of air
Φ_α spectral scaling parameter ($\equiv (\epsilon z)^{\frac{2}{3}}$); $\alpha = u, v, w$.

An overbar represents an average taken over one run unless otherwise stated. A prime signifies fluctuations. A quantity evaluated at the surface has a subscript zero.

TABLE 1. AIRCRAFT TURBULENCE INSTRUMENTATION

aircraft	parameter	recording resolution	sampling frequency/Hz	JASIN absolute accuracy† (r.m.s.)	primary instrument sources
C-130	u, v	0.05 m s^{-1}	20	±0.4 m s^{-1}	compensated pitot-static probe rotating sideslip vane INS/Doppler radar/Decca Navigator/Loran-C mix
	w	0.03 m s^{-1}	20	±0.1 m s^{-1}	compensated pitot-static probe rotating angle of attack vane INS/pressure altimeter mix
	T	0.006 K	20	±0.5 K‡	Rosemount open-wire platinum resistance thermometer
	q	0.02 g kg^{-1}	20	±0.5 g kg^{-1}‡	compensated pitot-static probe microwave refractometer E.G. & G. dew-point hygrometer Rosemount thermometer
	p	0.5 mbar	20	±1 mbar	compensated pitot-static probe
	z	0.8 m	2	±2%	radar altimeter
Electra	u, v	0.03 m s^{-1}	20	±0.6 m s^{-1}	Pitot-static probe fixed sideslip vane INS + C-130 position update
	w	0.01 m s^{-1}	20	±0.1 m s^{-1}	Pitot-static probe fixed angle of attack vane INS
	T	0.02 K	20	±0.5 K‡	Rosemount open-wire platinum resistance thermometer NCAR 'K-probe' open-wire thermometer pitot-static probe
	q	0.02 g kg^{-1}	20	±0.5 g kg^{-1}‡	Lyman α hygrometer E.G. & G. dew-point hygrometer
	p	0.5 mbar	20	±1 mbar	pitot-static probe
	z	0.08 m	20	±2%	radar altimeter
Falcon	u, v	0.05 m s^{-1}	100	not known	Rosemount 5-hole pressure probe INS
	w	0.01 m s^{-1}	100	±0.1 m s^{-1}	Rosemount 5-hole pressure probe INS
	T	0.025 K	100	±0.5 K‡	Rosemount open-wire platinum resistance thermometer
	q	0.01 g kg^{-1}	100	±0.5 g kg^{-1}‡	Lyman α hygrometer Väisälä humicap
	p	—	100	±1 mbar	
	z	—	100	±2%	radar altimeter

† During straight and level flight in cloud-free air (Nicholls & Cockcroft 1981).
‡ Biases were detected between the aircraft that stayed constant throughout the experiment. Differential accuracy is ±0.1 K and ±0.1 g kg^{-1}.

2. Instrumentation

The data presented in this paper were mainly obtained by three specially instrumented aircraft and two tethered balloon systems.

(*a*) *Aircraft*

The three participating aircraft (the MRF† C-130, NCAR† Electra and DFVLR† Falcon) were each capable of measuring all three wind components, temperature and humidity (means and fluctuations). Details of the mounting and location of the various sensors are contained in the summary by the Royal Society (1979).

The measurement of wind components from an aircraft is a two-stage process, the wind vector being the difference between the air motion relative to the aircraft and the aircraft motion relative to the Earth. Each aircraft is fitted with an inertial navigation system (INS), which specifies the attitude and velocity of the aircraft, with some form of pitot-static probe to determine the air speed. The wind vector may then be determined if the angles of attack or sideslip (or equivalent measures of the incident airflow) are measured. By these means the aircraft motion is entirely compensated for and the wind measurements are independent of any manoeuvres. Each aircraft does use slightly different measurement techniques; further details of these and other relevant measurements are contained in table 1.

More extensive information concerning these systems (frequency response, calibration, accuracy, data processing, operating procedures and additional instrumentation) may be found in Nicholls (1978, 1982), LeMone & Pennell (1980) and Royal Society (1977). At a typical air speed of 100 m s^{-1}, a 20 Hz sampling rate is equivalent to one measurement every 5 m along the track.

During JASIN, new procedures for correcting airborne wind measurements based on precision position-fixing information recorded by the C-130 were implemented. These have significantly improved the accuracy of the mean wind measurements made by the C-130 and the Electra, which error analysis (Nicholls 1982) shows to be about ± 0.5 m s^{-1} if the results of self-calibration manoeuvres are also included.

Numerous intercomparisons between the various instruments during the experiment have provided independent checks of data quality. Low-level flights past ships allowed comparisons with surface-mounted instrumentation (Nicholls 1982) while close-formation flying over long (60 km) distances allowed the aircraft systems to be compared (Nicholls & Cockcroft 1981; Nicholls *et al.* 1982). These reveal consistency of calibrations within the accuracies quoted in table 1, although the values for temperature and humidity contain a significant constant offset component. If this is removed by correction to a common standard, the relative accuracy is much higher (see the footnotes to table 1). Comparisons of fluctuation measurements made by the aircraft showed excellent agreement over most of the measured frequency range (10^{-3}–10 Hz) with only minor variations evident at the highest frequencies caused by slightly different noise characteristics. The frequency response of the aircraft systems is sufficient for accurate covariance measurements at all flight levels. The agreement between the aircraft variance and covariance measurements on intercomparison runs was again found to be very good and is particularly encouraging as the systems are completely independent and use a variety of different techniques.

† MRF, Meteorological Research Flight, U.K.; NCAR, National Center for Atmospheric Research, U.S.A.; DFVLR, Deutsche Forschungs- und Versuchsanstalt fur Luft- und Raumfahrt, F.R.G.

PHILOSOPHICAL TRANSACTIONS OF THE ROYAL SOCIETY A MATHEMATICAL, PHYSICAL & ENGINEERING SCIENCES

(*b*) *Tethered balloon systems*

Two tethered balloon systems were used during JASIN, one from the R.V. *Meteor*, the other from H.M.S. *Hecla*.

The *Meteor* system consisted of identical instrument packages suspended at three levels on the balloon cable with a fourth mounted on a boom extending from the bow of the ship. Measurements of mean and turbulent meteorological quantities were made from each package with the sensors listed in table 2. A device measuring visible radiation from ten different orientations was also included in each package to detect the presence of cloud.

TABLE 2. BALLOON-BORNE TURBULENCE INSTRUMENTATION

	parameter	sampling rate/Hz	resolution	accuracy	approximate sensor response/Hz	primary sensors
Meteor	u, v, w	2	0.01 m s^{-1}	±1% of mean	4‡	cup anemometer
		10	0.005 m s^{-1}			3D hot film,
		10	60 nT	$\overline{w} \equiv 0$	10	3D magnetometers
		10	0.005 m s^{-2}			and accelerometers
	T	10	0.003 K	0.1 K	10	platinum resistor
		2	0.01 K	0.1 K	1	thermistor
	q	2	0.01 K	0.1 K	1	wet thermistor
	p	10	0.025 mbar	0.1 mbar	10	Digiquartz
Hecla	u, v	10†	0.1 m s^{-1}	±2% of mean	5‡	cup anemometer
	w	10†	0.03 m s^{-1}	$\overline{w} \equiv 0$	30‡	hot-wire inclinometer
	T	10†	0.02 K	±0.2 K	10‡	platinum resistor
	q	10†	0.02 K	±1 g kg^{-1}	0.5‡	wet platinum resistor
	p	10†	0.1 mbar	±1 mbar	4	aneroid capsule

† After filtering at 4 Hz. ‡ In a windspeed of 5 m s^{-1}.

Motion of these packages due to ship and cable movement contaminates the wind measurements, especially at periods near 10 s, the frequency of the ship's motion. This was overcome by a correction procedure using measurements of the Earth's magnetic field and accelerometers contained in each package. In this way, most of the spurious contributions may be eliminated. Further details are contained in Brümmer & Wendel (1982). The system flown from *Hecla* carried a single probe to measure the parameters also listed in table 2. Cospectra derived from the probe data were cut off at a point where the effects of ship heave first became evident (0.09 Hz). Fluxes calculated from these were compensated for by the covariance lost at higher frequencies, standard cospectral shapes being assumed. Further details of instruments and results are given by Grant & Jenkins (1982).

3. THE DATA

Most of the aircraft data presented were obtained from box patterns flown at different levels in loose formation, as shown in figure 1. Patterns of this type were flown on eight days during JASIN in areas chosen for uniformity of conditions. The experimental parts of these flights were typically five–six hours long with measurements being made at a range of heights from 30 m above sea level upwards. Fluxes and other statistics were computed for each straight and level run (e.g. each side of a box) and, by averaging measurements made around the circumference of the boxes, quantities representative of an area roughly 70 km × 70 km

were obtained. These data therefore allow both vertical and horizontal gradients to be calculated accurately. In addition to these horizontal runs, profiles (ascents or descents) were flown to determine the gross structure of the boundary layer. These were also instrumental in determining the actual levels to be flown. Furthermore, where conditions permitted, the patterns were centred on a ship making simultaneous meteorological measurements.

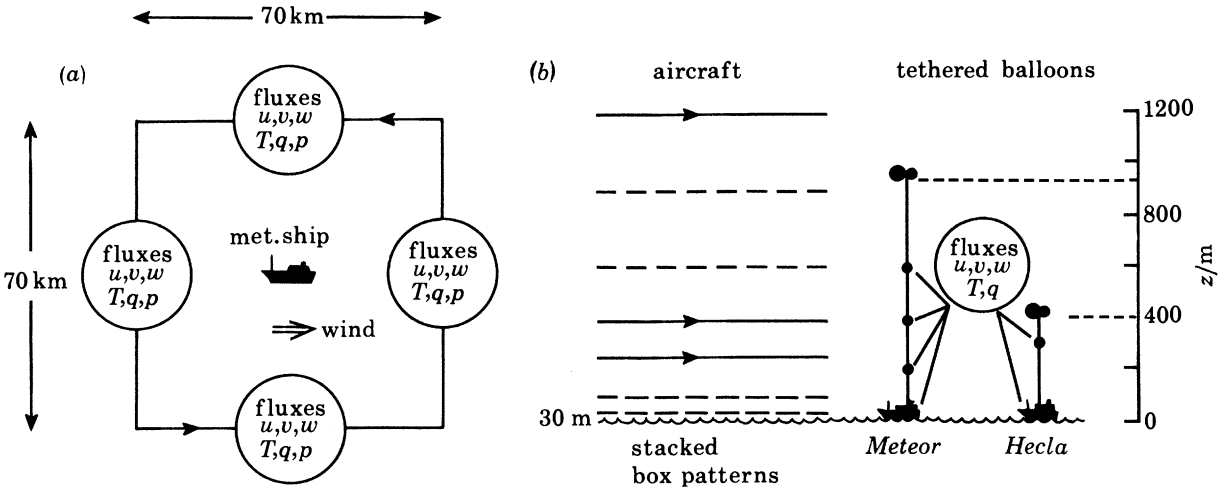

FIGURE 1. A typical flight pattern and deployment of instrumentation: (*a*) plan view; (*b*) side view. The important parameters measured are shown inside the circles.

The tethered-balloon observations were also used to measure turbulent fluxes and spectra, but generally on a smaller scale with time series up to one hour long. The balloons' ability to make simultaneous measurements at several levels facilitates the investigation of particular events, which might be lost in the larger-scale averaging inherent in the analysis of the aircraft data. The maximum altitudes attainable by the balloon systems are also shown in figure 1.

The strategy outlined enables data to be obtained on the effects of motions on scales up to approximately 70 km, corresponding to a timescale of a few hours. There is therefore a significant difference in scale between the radiosonde budget methods (Taylor *et al.* this symposium) and the results presented here.

4. General boundary layer structure

One of the outstanding features of JASIN was the large part of the time in which conditions were close to neutral stability, i.e. the heat and water vapour fluxes were very small throughout the boundary layer. Figure 2 shows a typical group of profiles. A well mixed layer extended from the surface to a height of 400–500 m, above which the virtual potential temperature Θ_v began to increase, tending to suppress dry turbulent mixing. At higher levels, on the particular occasion illustrated, an extensive sheet of stratocumulus was present. This cloud layer was also well mixed, as shown by the near-adiabatic increase of the liquid water content, Q_l. Mixing within the cloud is promoted by the destabilizing influence of the distribution of radiative heating and cooling (Slingo *et al.* 1982; Schmetz *et al.* this symposium), however, coupling

between the two mixed layers was observed to be weak and intermittent (this is discussed further in §7 below).

The types and amounts of boundary layer cloud (i.e. cumulus, stratocumulus and stratus) were observed to be variable during JASIN. This is compatible with profiles of the type shown in figure 2, where quite small changes in temperature or humidity (of only a few tenths of a degree or gram per kilogram) can lead to the formation or dissipation of cloud. Changes of this size were frequently detected across the flight patterns owing to larger-scale horizontal gradients.

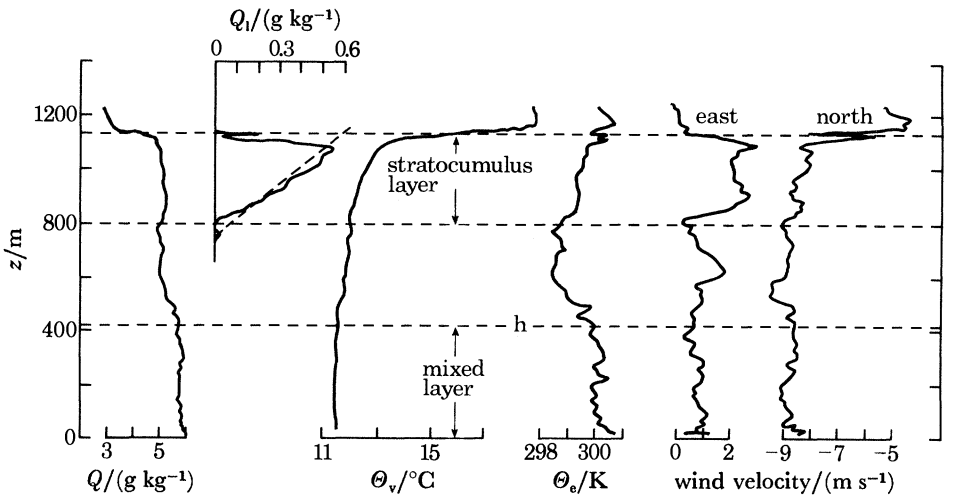

FIGURE 2. Profiles measured on descent by the C-130 at 11 h 15 G.M.T. on 7 August 1978. The dashed line on the Q_l-trace represents an adiabatic increase, the cloud base being assumed to be at 750 m.

Some results are now presented from a number of aircraft flights that took place in conditions like those outlined. Results from seven of the eight investigations are considered here, the other being stably stratified (i.e. having a negative surface buoyancy flux) and consequently having rather a different structure.

In all but this one stable case, a well mixed layer extending upwards from the surface was a common feature, but determining the depth from profile information like that shown in figure 2 proved very difficult because of the small departures from neutrality. Thus in the absence of well defined low-level inversions or other significant features, the mixed-layer depth, h, was defined from the momentum flux profiles. This has the additional advantage of being an area-averaged quantity, rather than being defined by a small number of profiles with the associated sampling problems.

When viewed in a coordinate system in which U is parallel to the surface wind, the $\overline{u'w'}$ component of the momentum flux was observed to decrease approximately linearly on each of the seven days chosen for analysis. The height at which a linear regression to the $\overline{u'w'}$ measurements became zero served to define h, a level that could often subsequently be identified with small discontinuities in the profiles (see for example figure 2). The other intercept provided a first estimate of the area-averaged surface stress, ρu_*^2 (these estimates were subsequently refined by using a better approximation to the observed flux profiles, as shown in figure 4). Values of the other surface fluxes and hence other scaling parameters (e.g. T_*, q_*) were obtained by similar methods (Nicholls 1982). Values of these surface fluxes are given in table 3. They

have been shown to be in reasonable agreement with the results of 'bulk aerodynamic' methods used concurrently during JASIN (Nicholls 1982).

The surface virtual heat or buoyancy fluxes are small but positive in each case. In more stable situations characterized by larger negative buoyancy fluxes, mixing is suppressed at low levels and large gradients may exist in layers close to the surface, which are not accessible to aircraft. (Under these conditions the stress measured at levels that are accessible to aircraft

TABLE 3. SURFACE FLUXES AND ASSOCIATED QUANTITIES DERIVED FROM AIRCRAFT MEASUREMENTS ON SEVEN CASE STUDIES

flight date (1978)	$-10^{-1}\overline{u'w'_0}$ / $(\mathrm{m\ s^{-1}})^2$	$10^{-3}\overline{w'T'_0}$ / $\mathrm{m\ s^{-1}\ K}$	$10^{-6}\overline{w'q'_0}$ / $\mathrm{m\ s^{-1}}$	$10^{-3}\overline{w'T'_{v0}}$ / $\mathrm{m\ s^{-1}\ K}$	$-L$ / m	h / m	hf/u_*	$-u_*/fL$	$-h/L$	symbol
28 Jul.	0.36	−0.5	7.0	0.7	710	240	0.16	2.1	0.3	□
29 Jul.	0.72	2.5	12.0	4.6	310	340	0.17	6.9	1.1	○
7 Aug.	0.49	12.0	14.0	14.4	54	410	0.26	32	7.6	▽
21 Aug.	1.30	2.0	13.0	4.3	790	450	0.16	3.6	0.6	●
23 Aug.	1.28	5.0	15.0	7.6	450	500	0.18	6.3	1.1	▲
25 Aug.	0.32	2.5	5.0	3.4	120	210	0.16	12	1.8	▼
31 Aug.	1.15	6.0	27.0	10.7	270	660	0.24	10	2.4	■

may be strongly modulated if the surface buoyancy flux changes sign owing, for example, to varying air or sea surface temperatures.) Values of the Monin–Obukhov length scale, L, are also given in table 3. Since $-L$ can be roughly interpreted as the height at which buoyant production of turbulent kinetic energy (TKE) exceeds shear production, only one occasion, 7 August, was relatively unstable ($-h/L \approx 8$). Table 3 also shows that the depth of the mixed layer, h, is approximately proportional to u_*/f, which is a prediction of neutral Ekman layer similarity theory (see for example Zilitinkevich 1972) with a constant of proportionality of about 0.2. This value is close to those generally quoted for neutral stability (0.25–0.3) (see reviews by McBean 1979, Tennekes 1973) and shows that under slightly unstable conditions the mixed layer does not necessarily extend to the lowest inversion base, which was generally at or above 1 km.

5. THE MOMENTUM AND TURBULENT KINETIC ENERGY BALANCE IN THE MIXED LAYER

If the momentum conservation equations are non-dimensionalized with velocity and length scales u_* and u_*/f, they may be written as

$$\frac{\partial(\overline{u'w'}/u_*^2)}{\partial(zf/u_*)} = \frac{1}{u_*}(V - V'_g), \tag{1}$$

$$\frac{\partial(\overline{v'w'}/u_*^2)}{\partial(zf/u_*)} = \frac{1}{u_*}(U'_g - U), \tag{2}$$

where the virtual geostrophic wind (U'_g, V'_g) is defined by

$$(U'_g, V'_g) = \left(-\frac{1}{f}\left(\frac{1}{\rho}\frac{\partial p}{\partial y} + \frac{\mathrm{D}V}{\mathrm{D}t}\right), \frac{1}{f}\left(\frac{1}{\rho}\frac{\partial p}{\partial x} - \frac{\mathrm{D}U}{\mathrm{D}t}\right)\right), \tag{3}$$

with

$$\frac{\mathrm{D}}{\mathrm{D}t} = u\frac{\partial}{\partial x} + v\frac{\partial}{\partial y} + w\frac{\partial}{\partial z} + \frac{\partial}{\partial t}.$$

Ekman layer similarity theory (see for example Clarke & Hess 1974, Tennekes 1973) predicts that provided the acceleration terms in equation (3) remain small, the functions defined in equations (1) and (2), i.e. the dimensionless flux profiles and the geostrophic departure (or velocity defects), should be universal functions of only the dimensionless height, zf/u_*, in neutral, barotropic conditions. This provides a general framework for the analysis of the observations as a whole, rather than a series of case studies.

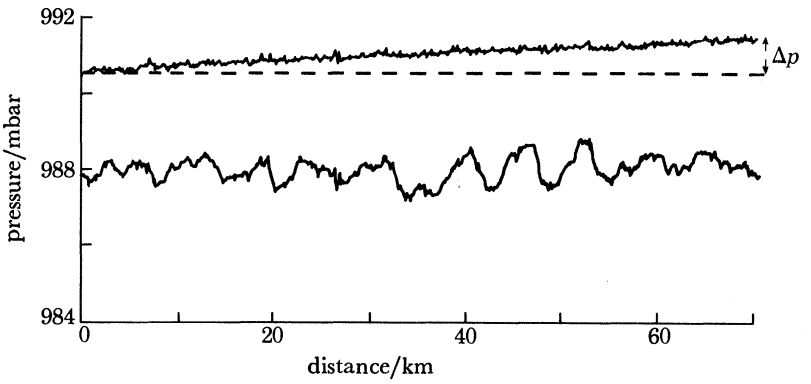

FIGURE 3. Horizontal pressure gradients measured by the *Electra* before (lower curve) and after (upper curve) correction for altitude variations. The resulting pressure difference, Δp, obtained by linear regression was subsequently used in geostrophic wind calculations.

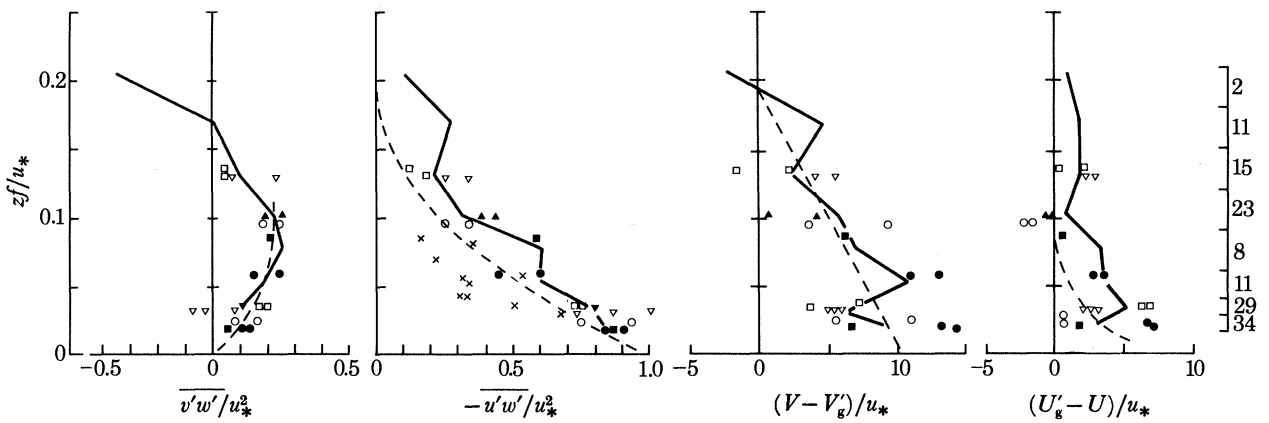

FIGURE 4. Scaled momentum flux and velocity defect profiles. The symbols represent averages from aircraft data from particular days (see table 3). Tethered balloon data are denoted by crosses. The solid curves connect mean values for dimensionless height classes (aircraft data only). The extent of these classes and the number of observations in each appear at the right of the figure. The dashed curves are explained in the text.

Each of the terms in equations (1) and (2) has been evaluated by using aircraft data (Nicholls 1982). Best-fit horizontal gradients for the whole mixed layer were determined for each occasion by multiple regression with use of the differences measured along each of the runs. Pressure gradients were determined from pressure and radar altimeter measurements as illustrated in figure 3. Furthermore, as the number of runs completed on each occasion averaged 20, the horizontal gradients of pressure, velocity components, temperature and humidity representative of a 70 km × 70 km area could be determined quite accurately. The standard error in the geostrophic wind determinations was generally a few tenths of 1 m s^{-1}. The virtual tem-

perature gradients showed baroclinity was small, and the velocity gradients enabled layer-averaged acceleration terms to be determined although the local rate of change was determined from surface measurements from ships.

The momentum flux and velocity defect profiles are shown in figure 4. The symbols represent the average from each particular box pattern, but since these only make up 70% of the total available data, the results as a whole have also been grouped into non-dimensional height classes as shown in the figure. The momentum flux profiles are well defined with little scatter, suggesting they are not significantly affected by the small departures from neutrality listed in table 3. Also shown in this figure are points from the tethered balloon measurements (Grant & Jenkins 1982) during the period 23–25 August when conditions were neutral or slightly stable at the northeast corner of the JASIN meteorological triangle. The generally lower values may be due to the difference in stability, but could also be explained by different methods of assessing u_*.

The measured near-surface stress and wind are closely parallel (since $\overline{v'w'} \approx 0$ there) and the $\overline{u'w'}$ component decreases to become small near $\hat{z}\ (\equiv zf/u_*) \approx 0.2$ as mentioned earlier. The velocity defects are more scattered, but show that the main effect of the momentum transfer is to turn the wind with height ($V - V'_g > U'_g - U$). At $\hat{z} \approx 0.2$, the velocity defects approach zero as the effects of turbulent momentum transfer are diminished. The balance between the momentum fluxes and velocity defects is shown by the dashed curves. Those drawn on the momentum flux profiles have been obtained by integrating the curves drawn through the velocity defect data upwards from the surface. Those drawn on the velocity defect profiles were defined by linear regression for the $(V - V'_g)/u_*$ data, but the scatter of the other component is larger and a better constraint was provided through the TKE balance discussed below. Within the limits set by experimental error, the balance shown in figure 4 is quite good at all levels although the decrease in $\overline{v'w'}/u_*^2$ observed in the upper half of the mixed layer would require negative values of $U'_g - U$ if equation (2) was to balance exactly. As the winds were not observed to be consistently supergeostrophic, this suggests that the flow aloft must have been accelerating relative to that at lower levels. This is perhaps to be expected, as the atmosphere is in a state of constant adjustment and the time required for a close balance to be achieved is likely to be of the order of $2\pi f^{-1}$ ($\approx$ 14 h at 60° N), especially at higher levels in the mixed layer (see for example Mason & Sykes 1980).

Ekman similarity theory predicts that the profiles shown in figure 4 should be universal functions under steady, neutral, barotropic conditions and in particular should be independent of surface characteristics as long as $z \gg z_0$ and the surface Rossby number, G/fz_0 is large (see for example Tennekes 1973). Since $z_0 \approx 10^{-4}$ m during JASIN (Nicholls 1982), $G/fz_0 \approx 10^9$, so both conditions are likely to be fulfilled at all measurement levels. Comparisons with the only previously published experimentally determined neutral wind defect profiles (Clarke & Hess 1974) are shown in figure 5. These were obtained from pilot balloon ascents at an overland site in Australia ($G/fz_0 \approx 5 \times 10^7$) (Hess *et al.* 1981). There is a reasonable measure of agreement given the differences in techniques and the difficulties encountered in that experiment of obtaining representative spatially averaged data (Clarke & Hess 1974, Hess *et al.* 1981). Also shown in figure 5 are two solutions obtained from numerical simulations of neutral conditions with a three-dimensional model (Deardorff 1972) and a one-dimensional second-order closure model (Wyngaard *et al.* 1974). Close agreement is observed in all but the $\overline{v'w'}/u_*^2$ profiles. This illustrates an important difference between ideal steady, neutral solutions and those

PHILOSOPHICAL TRANSACTIONS OF THE ROYAL SOCIETY A MATHEMATICAL, PHYSICAL & ENGINEERING SCIENCES

likely to be observed in the atmosphere, even though the observations were made in very nearly neutral conditions. This difference is basically due to the weak stratification that exists above the mixed layer (as seen in figure 2), which is sufficient to suppress the turbulent mixing, driving both components of the momentum flux to zero at the same level. This can be investigated further by examining the TKE balance.

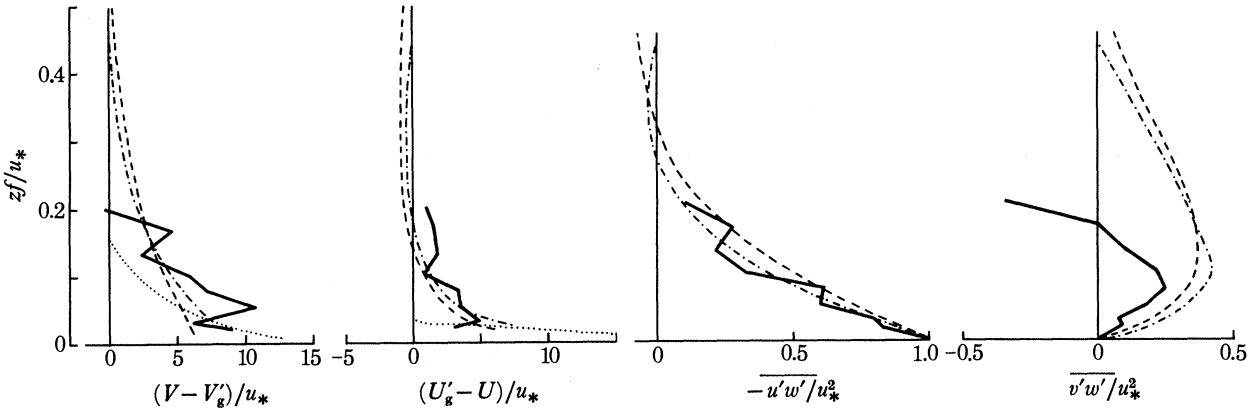

FIGURE 5. Comparisons of scaled momentum flux and velocity defect profiles with previous experimental and numerical results. ——, JASIN data (as figure 4); . . . . ., experimental data from Clarke & Hess (1974); – – – –, – · – · –, theoretical results from the numerical models of Wyngaard *et al.* (1974) and Deardorff (1972) respectively.

The scaled TKE balance may be expressed in the form

$$\frac{1}{u_*^2 f}\frac{\partial \bar{E}}{\partial t} = \frac{1}{k}\left(\frac{-u_*}{fL}\right)\left(\frac{\overline{w'T_v'}}{\overline{w'T_{v,0}'}}\right) - \frac{\partial}{\partial \hat{z}}\left(\frac{\overline{w'p'}}{\rho u_*^3} + \frac{\overline{w'E}}{u_*^3}\right) - \overline{u'w'}\frac{\partial (U/u_*)}{\partial \hat{z}} - \overline{v'w'}\frac{\partial (V/u_*)}{\partial \hat{z}} - \frac{\epsilon}{u_*^2 f}. \qquad (4)$$

O B C T S1 S2 D

Each of these terms may be derived from aircraft measurements with the exception of C (see for example Pennell & LeMone 1974, Lenschow *et al.* 1980). The measurements show that term O is negligibly small. The shear production terms S1 and S2 could be derived directly from the results shown in figure 4 (since the geostrophic wind shear is small compared with the actual wind shear) but the scatter in the $(U_g'-U)/u_*$ measurements precludes any accurate determination of S1. Thus it was decided to obtain S1 as a residual by assuming C to be negligible. Previous experimental and numerical studies indicate that this assumption can be justified provided levels close to the surface are avoided (Lenschow *et al.* 1980, Deardorff 1974, Lenschow 1974). The dissipation rate, term D, was estimated from the inertial subrange of the one-dimensional vertical velocity spectra with use of a Kolmogorov constant of $\frac{4}{3} \times 0.5$ (see for example Nicholls & Readings 1981). The buoyancy term, B, is a product of the normalized virtual heat flux and the stability parameter (u_*/fL).

The variation of each of these terms with height is shown in figure 6, which shows best-fit curves to data taken from all but the most unstable day, 7 August, in which a significantly different balance was observed. Unlike many previous results (see for example Lenschow *et al.* 1980, Caughey & Wyngaard 1979) both terms B and T are small throughout the mixed layer and self-cancelling to some extent. This implies that most of the shear production of TKE, the dominant production term throughout much of the mixed layer, is dissipated locally (S1 shown in figure 6 was used to calculate values of the velocity shear and hence the profile drawn

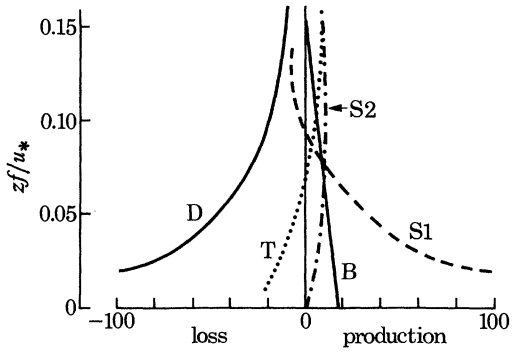

FIGURE 6. Variation of terms of the scaled TKE budget with height. The terms are given in equation (4).

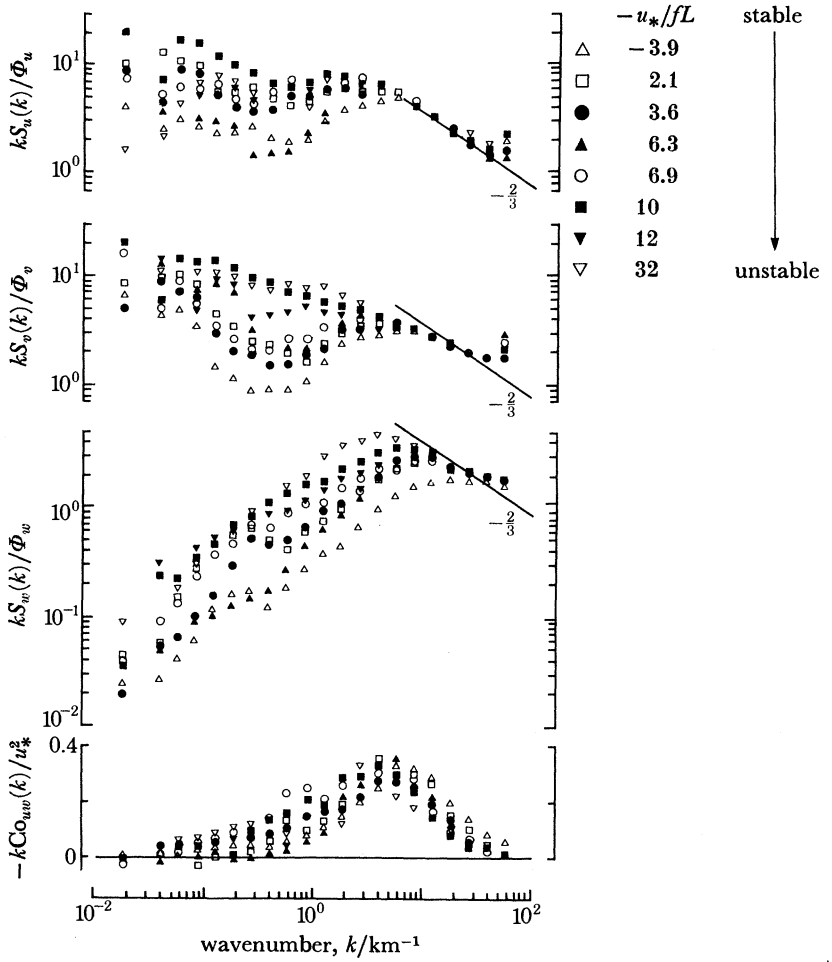

FIGURE 7. Average velocity spectra and *uw* cospectra from low-level ($zf/u_* \approx 0.02$) aircraft data. Symbols are as listed in table 3; △ is for the additional stable case. Values of the stability parameter $-u_*/fL$ for each symbol are also shown.

on the $(U'_g - U)/u_*$ data in figure 4). Term D decreases by an order of magnitude through the mixed layer, and at the higher levels all the terms become small and roughly the same size as the uncertainty involved in their determination. With such small transport and production terms, the degree of turbulent mixing at these levels remains very sensitive to small changes in stratification, and turbulence could be suppressed even by very weak density gradients.

6. Mixed-layer spectra

The turbulent fluctuation data from both aircraft and balloons were investigated by using spectral analysis (fast Fourier transform techniques). Those derived from aircraft data cover a much wider bandwidth (as the airspeed is about 100 m s^{-1}). Figure 7 shows average velocity spectra from aircraft data obtained at low level ($\hat{z} \approx 0.02$) on eight occasions: the seven discussed above plus the stably stratified case. The data are two-dimensional averages, i.e. they contain data from along- and across-wind-sampled runs around box patterns. Although differences have been shown to exist at low levels between spectra sampled in this way (Nicholls & Readings 1981), their effects on the averaged spectra presented here are small, especially when compared with the features discussed below. The spectra have been brought into coincidence at high wavenumbers and are plotted on a double logarithmic scale as $kS_x(k)$ against k (after Kaimal *et al.* 1972). All show an approach towards the expected $-\frac{2}{3}$ power-law behaviour at high wavenumbers although the combined effects of noise and aliasing are visible at the highest wavenumbers.

The spectra generally reveal two ranges of wavenumbers that contain a relatively large proportion of the total variance. In figure 7 both the u and the v spectra display minima at $k \approx 0.4$ km^{-1} although this becomes less distinct with increasing instability (as measured by the stability parameter $-u_*/fL$). This minimum is even more pronounced in the temperature and humidity spectra (Nicholls 1982), which are more strongly bimodal. By contrast, the w spectra are singly peaked so that at high wavenumbers the partition of energy between the three velocity components is approximately equal while the motion at low wavenumber is strongly two-dimensional.

The peaks of the regions of the spectra of high wavenumber ($k > 0.4$ km^{-1}) tend to move to lower wavenumbers as instability increases in agreement with previous findings (see for example Kaimal *et al.* 1972). The same happens at higher levels in the mixed layer, although the most noticeable effect is the reduction in amplitude of the high wavenumber part of the u, v, T and q spectra relative to the contributions from the low wavenumber end. The latter tend to remain unchanged throughout the mixed layer and therefore dominate the overall variance at higher levels.

The fluxes are confined almost entirely to the high wavenumber region as illustrated by the uw cospectra in figure 7. This is confirmed by the tethered balloon results of Grant & Jenkins (1982). Thus the fluxes discussed earlier seem to be representative of the effects of small-scale turbulent mixing, which decreases in intensity with height within the mixed layer and responds to changes in the mixed-layer stability parameter, u_*/fL. This appears to be superimposed on a larger (more than 10 km) scale variability, which does not scale in the same way and is probably not associated with the same physical processes.

7. Interaction between the mixed layer and cloud

Previous sections have indicated that, when averaged over a wide area, small-scale turbulent mixing becomes much reduced at $\hat{z} \approx 0.2$. However, some transport out of the mixed layer was regularly observed in the form of cumulus convection. This is consistent with the requirements of a balanced water vapour budget within the mixed layer where water vapour supplied by the positive surface fluxes (see table 3) must be removed if the mixed layer is not to become

saturated, which was not observed. This may be accomplished by large-scale horizontal divergence, growth of the mixed layer upwards or transport out of the mixed layer. The radiosonde budgets (Taylor *et al.* this symposium) show that horizontal divergence alone is insufficient and that significant water vapour transport occurs above the mixed layer and throughout the cloud layer. This suggests that cumulus convection is responsible.

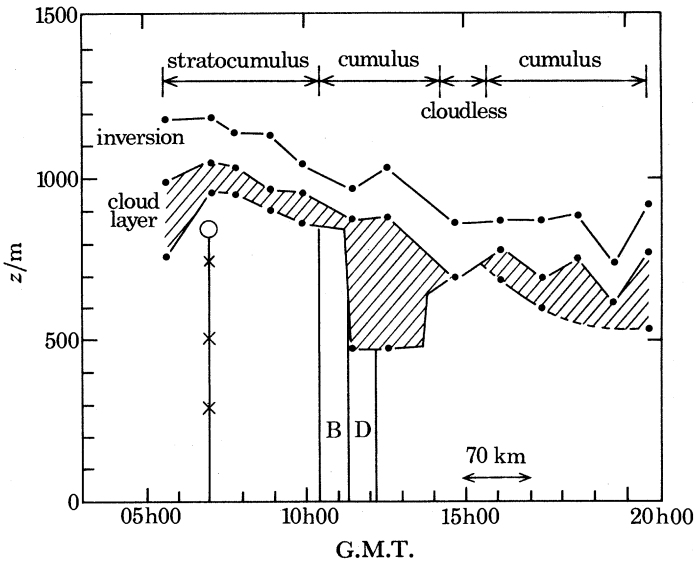

FIGURE 8. Time series of inversion heat and cloud structure observed from *Meteor* on 1 Sep. 1978. The heights of the turbulence instrumentation are marked by crosses. An equivalent distance scale calculated from the observed 10 m wind is also shown.

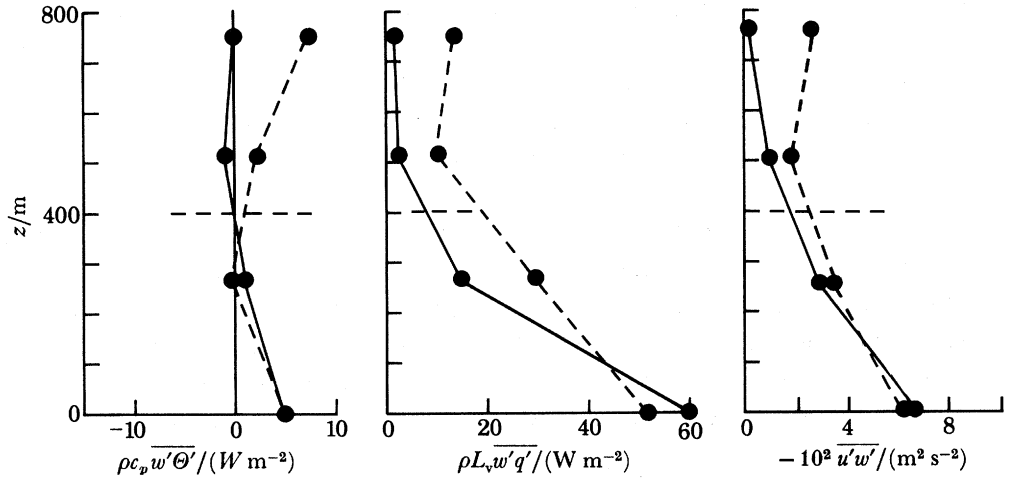

FIGURE 9. Flux profiles measured at *Meteor* before (——) and during (– – –) the passage of the cumulus cloud field. Horizontal dashed line indicates the mixed-layer depth.

Cloud formation depends upon mixed-layer air reaching its lifting condensation level (LCL), and cumulus will form if the upper levels are conditionally unstable (i.e. if Θ_e decreases with height). An example is shown in figure 2, where the LCL is *ca.* 360 m, the foregoing conditions are satisfied and a field of cumulus extending into the overlying stratocumulus was observed. With profiles like these the onset of cumulus convection is clearly very sensitive to small changes

in the mixed-layer temperature and humidity structure and to slight variations in the Θ_e profiles. In addition, cloud formation could display periodicity in some circumstances, for if there is initially no cloud and no removal of water vapour from the mixed layer, the associated moistening will lower the LCL and increase the low-level Θ_e making cumulus convection more likely. Subsequent cloud formation may then transport sufficient moisture upwards to lift the LCL again.

Thus cumulus cloud was generally observed to be intermittent and irregularly distributed on scales of tens of kilometres. This is illustrated in figure 8, which shows a time series observed at *Meteor*. The cumulus field observed at 11h 20 G.M.T. was associated with a slight cooling (0.1 K) and moistening (0.2 g kg^{-1}) throughout the mixed layer, which lowered the LCL sufficiently for cumulus to form. Turbulence data were obtained at the three levels indicated and at the surface during the intervals marked B and D (i.e. before and during the passage of the cloud field). The corresponding flux profiles are shown in figure 9. These indicate enhanced heat and water vapour transport in the upper mixed layer and above. The mixed-layer depth was estimated to be between 400 m and 500 m from thermodynamic and momentum flux profiles while $0.2\,u_*/f \approx 400$ m. Spectral analysis of these data revealed considerably increased variance and covariance on kilometre scales. This agrees with aircraft results, where large water vapour fluxes (but not momentum fluxes) were sometimes measured on single runs near the top of the mixed layer. The tethered balloon data therefore imply that transport above $\hat{z} \approx 0.2$ is strongly dependent on the presence of cloud and shows that the surrounding regions are essentially non-turbulent. These cloud processes are associated with very different scales from those of the mixing processes that predominate within the mixed layer, and may contribute to the variability observed at low wavenumbers in the mixed-layer spectra. Although many plausible physical mechanisms can be postulated that might affect the thermodynamic structure of the boundary layer on these larger scales (and therefore the cloud structure), the data presented here cannot address those questions directly.

8. Concluding remarks

This paper has given an overall impression of the mixing processes observed during JASIN and their effects on and relation to the structure of the atmospheric boundary layer. Within this framework, further investigations are proceeding into the response of the turbulent mixing to specific mesoscale events. Also further work is being undertaken in studying the anisotropy of shear layer turbulence through the variation of the orientation of the principal axes of the measured stress tensor (Fiedler & Hafner 1983). This has been shown to vary consistently with changing stability, but is not well predicted by present second-order closure models.

The results presented here from aircraft and tethered balloon data are typical of the conditions that persisted throughout much of the JASIN experiment. It is not surprising that conditions of nearly neutral stability were encountered with such regularity, since the sea–air temperature difference in this part of the world is usually very small for much of the summer. Figures taken from Ocean Weather Station I at 59° N, 19° W show this difference to be between 0 K and +1 K for 50% of the time during July and August (Royal Society 1977) (statistics cover the years 1949–64).

Results obtained mainly from a series of studies with aircraft data in slightly unstable con-

PHILOSOPHICAL TRANSACTIONS OF THE ROYAL SOCIETY A MATHEMATICAL, PHYSICAL & ENGINEERING SCIENCES

ditions revealed a mixed layer extending from the surface to a height of approximately $0.2\ u_*/f$, considerably lower than the levels of the lowest inversion bases. Furthermore, by using the framework of Ekman similarity theory, the momentum flux and velocity defect profiles were shown to balance quite successfully, so the scaled profiles should be generally representative of neutral, barotropic Ekman layers. Differences between these results and theoretical solutions appear to reflect the presence of the weakly stable layer above the mixed layer, which was still sufficient to suppress turbulent mixing there. This finding is supported by the analysis of the TKE balance, which shows that the turbulent transport and buoyancy terms are small throughout the mixed layer, implying that the main shear production term is dissipated locally. Thus the intensity of the turbulence becomes small near the top of the mixed layer.

Spectral analysis of turbulent fluctuation data in the mixed layer reveals that the energy is mostly contained in two ranges of wavenumbers. Turbulent fluxes are mainly confined to the higher wavenumber part, which scales with the mixed-layer depth and stability parameters. The low wavenumber part generally contains the larger proportion of the variance (except for vertical velocity) and tends to remain unchanged with height within the mixed layer.

Transport of heat and water vapour from the mixed layer is strongly dependent on the presence of cloud, which locally enhances mixing in the upper mixed layer. Cloud was generally observed to be irregularly distributed on scales of tens of kilometres, indicating that turbulent transport changes markedly from continuous, small-scale mixing dominant within the mixed layer to much more intermittent processes above, characterized by significantly larger scales.

A variety of physical processes could give rise to variability on these larger scales, but they will require further detailed study.

We would like to thank everyone involved in the design, execution and analysis of the JASIN experiment, who made it a pleasurable and rewarding experience. Our particular thanks go to those who flew the aircraft and who manned the ships together with our colleagues at the various institutions involved without whom this work would not have been possible.

References

Brümmer, B., Augstein, E. & Riehl, H. 1974 On the low level wind structure in the Atlantic trade. *Q. Jl R. met. Soc.* **100**, 109–121.

Brümmer, B. & Wendel, M. 1982 Flux measurements with a tethered balloon system during the passage of a mesoscale field of low level cumulus clouds.

Busch, N. 1973 *Workshop on micrometeorology*, pp. 1–66. Boston: Am. Met. Soc.

Businger, J. A. 1973 *Workshop on micrometeorology*, pp. 67–100. Boston: Am. Met. Soc.

Caughey, S. J. & Palmer, S. G. 1979 Some aspects of structure through the depth of the convective boundary layer. *Q. Jl R. met. Soc.* **105**, 811–828.

Caughey, S. J. & Wyngaard, J. C. 1979 The turbulence kinetic energy budget in convective conditions. *Q. Jl R. met. Soc.* **105**, 231–240.

Clarke, R. H. & Hess, G. D. 1974 Geostrophic departure and the functions A and B of Rossby-number similarity theory. *Boundary-Layer Met.* **7**, 267–287.

Deardorff, J. W. 1972 Numerical investigation of neutral and unstable planetary boundary layers. *J. atmos. Sci.* **29**, 91–115.

Deardorff, J. W. 1974 Three dimensional study of turbulence in an entraining mixed layer. *Boundary-Layer Met.* **7**, 199–226.

Fiedler, F. & Hafner, T. 1983 Turbulent momentum transport and the structure of eddies. (In preparation.)

Grant, A. & Jenkins, G. 1982 Tethered balloon turbulence probe measurements from HMS *Hecla* during JASIN 1978. Meteorological Office Internal note TDN136.

Hess, G. D., Hicks, B. B. & Yamada, T. 1981 The impact of the Wangara experiment. *Boundary-Layer Met.* **20**, 135–174.

PHILOSOPHICAL TRANSACTIONS OF THE ROYAL SOCIETY A MATHEMATICAL, PHYSICAL & ENGINEERING SCIENCES

Kaimal, J. C., Wyngaard, J. C., Haugen, D. A., Cote, O. R., Izumi, Y., Caughey, S. J. & Readings, C. J. 1976 Turbulence structure in the convective boundary layer. *J. atmos. Sci.* **33**, 2152–2169.
Kaimal, J. C., Wyngaard, J. C., Izumi, Y. & Cote, O. R. 1972 Spectral characteristics of surface layer turbulence. *Q. Jl R. met. Soc.* **98**, 563–589.
LeMone, M. A. & Pennell, W. T. 1980 A comparison of turbulence measurements from aircraft. *J. appl. Met.* **19**, 1420–1437.
Lenschow, D. H. 1974 Model of the height variation of the turbulence kinetic energy budget in the unstable planetary boundary layer. *J. atmos. Sci.* **31**, 465–474.
Lenschow, D. H., Wyngaard, J. C. & Pennell, W. T. 1980 Mean-field and second moment budgets in a baroclinic, convective boundary layer. *J. atmos. Sci.* **37**, 1313–1326.
Mason, P. J. & Sykes, R. I. 1980 A two-dimensional numerical study of horizontal roll vortices in the neutral atmospheric boundary layer. *Q. Jl R. met. Soc.* **106**, 351–366.
McBean, G. A. (ed.) 1979 The planetary boundary layer. *Tech. Notes Wld met. Org.*, no. 165.
Nicholls, S. 1978 Measurement of turbulence by an instrumented aircraft in a convective atmospheric boundary layer over the sea. *Q. Jl R. met. Soc.* **104**, 653–676.
Nicholls, S. 1982 An observational study of the marine atmospheric boundary layer. Ph.D. thesis, University of Southampton.
Nicholls, S. & Cockroft, P. E. 1981 Intercomparisons between aircraft during JASIN: averaged measurements. MRF Internal note no. 10.
Nicholls, S. & Readings, C. J. 1981 Spectral characteristics of surface layer turbulence over the sea. *Q. Jl R. met. Soc.* **107**, 591–614.
Nicholls, S., Shaw, W. J. & Hauf, T. 1982 An intercomparison of aircraft turbulence measurements made during JASIN. *J. appl. Met.* (Submitted.)
Pennell, W. T. & LeMone, M. A. 1974 An experimental study of turbulence structure in the fair-weather trade wind boundary layer. *J. atmos. Sci.* **31**, 1303–1323.
Royal Society 1977 *Air–sea interaction project. Scientific plans for 1977 and 1978.*
Royal Society 1979 *Air–sea interaction project. Summary of the 1978 field experiment.*
Slingo, A., Nicholls, S. & Schmetz, J. 1982 Aircraft observations of marine stratocumulus during JASIN. *Q. Jl R. met. Soc.* **108**.
Tennekes, H. 1973 *Workshop on micrometeorology*, pp. 177–216. Boston: Am. Met. Soc.
Wyngaard, J. C. 1973 *Workshop on micrometeorology*, pp. 101–149. Boston: Am. Met. Soc.
Wyngaard, J. C., Cote, O. R. & Rao, K. S. 1974 Modelling the atmospheric boundary layer. *Adv. Geophys.* **18 A**, 193–211.
Zilitinkevich, S. S. 1972 On the determination of the height of the Ekman boundary layer. *Boundary-Layer Met.* **3**, 141–145.

Discussion

P. K. Taylor (*Institute of Oceanographic Sciences, Brook Road, Wormley, Godalming, Surrey GU8 5UB, U.K.*). Mr Nicholls has shown that the aircraft-measured turbulent momentum flux in the surface wind direction was small in the region of the cloud base. However, by calculating momentum budgets over the 200 km side JASIN triangle for periods of 12–20 hours, Taylor *et al.* (this symposium) have concluded that there was significant sub-grid-scale momentum transfer through the cloud base and through much of the cloud layer. The tethered-balloon stress values just above the cloud base were small before the passage of a cumulus cloud field but rose to about one third of the surface flux value during that passage. Is it possible that the difference between the aircraft measurements and the large-scale budgets is due to the aircraft's having preferentially sampled regions in which cumulus convection was not present beneath the stratocumulus? If so, and if the cumulus convection is an intrinsic part of the boundary layer, being needed for example to remove water vapour from the subcloud layer, then perhaps the aircraft results do not describe an important aspect of the boundary layer structure.

It should be recalled that the uncertainties inherent in flux profiles derived from budget

S. Nicholls. The correct interpretation of the results obtained by these different methods requires a careful assessment of both the accuracy and the representativeness of the measurements.

residuals are considerable owing to the cumulative errors incurred in integration from a surface value prescribed by a bulk parametrization. In contrast, the aircraft momentum fluxes are derived by eddy-correlation, have been shown to give excellent agreement with bulk parametrization formulae and are observed to respond to even quite small changes in the mean flow measured across the 70 km × 70 km experimental areas.

Indeed, the only reason that the budget-derived momentum fluxes decrease to zero at all is because of corrections made to the measured pressure field, which force this to happen. Taylor *et al.* (this symposium) argue that the application of these pressure field corrections represents the most reasonable interpretation of the budget data, since forcing the stress to zero at lower levels (thus giving closer agreement with the aircraft results) would require larger corrections.

If it is assumed that these corrected budget-derived profiles are free from serious error, then the question becomes one of representativeness.

Here, the difference in scales of the budget and aircraft measurements must be considered. A budget residual represents the integrated effect of *all* small-scale transport processes occurring within the 200 km side JASIN triangle over 12–20 hours. It may also yield spurious 'sub-grid' fluxes caused by nonlinear variation of the fields between the observation points during this time, which are indistinguishable from the effects of real small-scale transport. The aircraft were more selective, choosing to obtain area-averaged measurements representative of a smaller area over a correspondingly shorter time. These momentum fluxes were shown to balance quite well with the independently determined ageostrophic terms. Only a limited number of occasions (seven) could be investigated, and they all turned out to be close to neutral stability, possibly as a result of preferential sampling of areas that appeared to be more homogeneous, although such conditions were typical of those encountered throughout the experiment. Cumulus convection was observed from the aircraft on four of these occasions although often of limited vertical and horizontal extent.

Given the degree of spatial variability observed in the JASIN area, it is quite likely that the areas sampled by the aircraft were not representative of the conditions coexisting within the entire 200 km side JASIN triangle, nor do we claim this to be the case, just as the budget 'sub-grid' flux profiles are not representative of the area explored by the aircraft, or indeed any other area of similar size.

Therefore, I believe that the difference between the results obtained by these two methods reflects a combination of their different scales and the scale of the observed variability. Rather than considering the aircraft results as having failed to describe an important aspect of boundary layer structure, it should be reognized that both techniques have their strengths and weaknesses: the budget results reflect the integrated effect of changes in local conditions, e.g. enhanced wind speed, instability or cloud cover, whereas the aircraft investigate the relation of the mixing processes to a much better-defined local mean flow in considerable detail, but may not encompass the same range of conditions. One of the important features of JASIN was that both methods could be used together.

Finally, the question also implies that transport of water vapour from the mixed layer by cumulus cloud is accompanied by a corresponding transport of momentum. This may not necessarily be true, since the mean vertical wind and humidity gradients are generally different. Large upward water vapour fluxes were occasionally measured by the aircraft at the top of the mixed layer without a corresponding increase in the momentum fluxes. Also, the decrease of

PHILOSOPHICAL TRANSACTIONS OF THE ROYAL SOCIETY A MATHEMATICAL, PHYSICAL & ENGINEERING SCIENCES

momentum flux with height was usually observed to be much more rapid than that of the water vapour flux, implying that significant water vapour fluxes at upper levels were usually associated with small momentum fluxes.

J. A. Businger (*Department of Atmospheric Sciences, University of Washington, Seattle, Washington* 98195, *U.S.A.*). To organize the data Mr Nicholls used as non-dimensional height zf/u_* instead of the allegedly more suitable z/z_i for convective boundary layers. Can he explain why he prefers to use u_*/f as the scaling height?

S. Nicholls. First, the JASIN boundary layer investigated here was not particularly convective, in fact a better description is near-neutral. This is reflected in the values of the ratio $-h/L$ (where h is the mixed-layer depth), which were near unity. In the convective boundary layer referred to, this parameter is generally at least an order of magnitude larger.

Second, $z_i/h > 1$ on each occasion so the height of the mixed layer was not constrained by a low-level inversion.

Under these two conditions, there is clearly a close approximation to neutral stratification at low levels, where the theoretical expectation is for the scale height to be u_*/f. This was confirmed by the observations, in which h was found to be approximately $0.2\, u_*/f$.

The surface buoyancy fluxes were sufficiently small that the mixed layer could not deepen until constrained by z_i. In fact there were several occasions in which a stratocumulus mixed layer was observed just below z_i that was distinct from the mixed layer adjacent to the surface. In such a situation it is very unlikely that z_i would be a relevant height scale in either mixed layer. On other occasions it was also clear that small-scale turbulent mixing did not extend continuously from the surface to z_i, but to h instead.

J. D. Woods (*Institut für Meereskunde, Düsternbrooker Weg* 20, *D*-2300 *Kiel, F.R.G.*). Do the measurements made by aircraft or tethered balloons tell us anything about the diurnal variation in the atmospheric boundary layer during JASIN?

S. Nicholls. They tell us very little. This was not one of the stated objectives of the various measurement programmes so almost all of the data were collected during the day and, by aircraft, around local noon. A very small amount of nocturnal tethered balloon data does exist, but this does not constitute a significant sample.

PHILOSOPHICAL TRANSACTIONS OF THE ROYAL SOCIETY A MATHEMATICAL, PHYSICAL & ENGINEERING SCIENCES